

# Near and Mid Infrared Imaging Polarimetry of NGC1068

S.L. Lumsden<sup>1</sup>, T.J.T. Moore<sup>2</sup>, C. Smith<sup>3</sup>, T. Fujiyoshi<sup>3</sup>, J. Bland-Hawthorn<sup>1</sup>  
and M.J. Ward<sup>4</sup>

<sup>1</sup> Anglo-Australian Observatory, PO Box 296, Epping, NSW 2121, Australia  
*Email – sll@aoepp.aao.gov.au, jbh@aoepp.aao.gov.au*

<sup>2</sup> Astrophysics Research Institute, Liverpool John Moores University, Byrom Street, Liverpool L3 3AF  
*Email – tjtm@staru1.livjm.ac.uk*

<sup>3</sup> School of Physics, University College UNSW, Australian Defence Force Academy, Canberra 2600, Australia  
*Email – craig@phadfa.ph.adfa.oz.au, txf@phadfa.ph.adfa.oz.au*

<sup>4</sup> University of Leicester, Department of Physics and Astronomy  
*Email – mjw@star.le.ac.uk*

1 November 2018

## ABSTRACT

We present the results of a series of observations of the near- and mid-infrared polarisation properties of the Seyfert 2 galaxy NGC1068. Our data agree well with previously published results in showing the need for a separate polarisation mechanism in the near infrared apart from scattering. We find that the predictions of a simple model in which this component arises through absorptive dichroism due to aligned grains within the extended warm ( $\sim 400\text{K}$ ) dust fits the data reasonably if the obscured background source is itself due to dust emission (at temperature  $> 1000\text{K}$ ). By considering the change of polarisation with wavelength we show that the extinction to this hot dust region is in the range  $A_V = 20 - 40$ . Consideration of the observed data then leads us to the conclusion that if viewed face-on, NGC1068 would have a strong near-infrared excess similar to Seyfert 1 galaxies. Comparison with other independent measures of the extinction to the active nucleus itself lead us to the conclusion that the hot dust must provide screening equivalent to at least  $A_V = 40$ , and possibly much higher. We speculate that this component alone may be the ‘classical’ torus discussed in terms of the unified model, and the more extensive mid-infrared emission may arise from circumnuclear molecular cloud material, and dust in the ionisation cones.

**Key words:** galaxies: individual (NGC1068) – galaxies: Seyfert – galaxies: nuclei of – infrared: galaxies – galaxies: active – polarisation

## 1 INTRODUCTION

The unified model for Seyfert galaxies proposes that all types of Seyfert galaxy are basically the same, but that a dusty molecular ‘torus’ obscures the broad-line region (BLR) in many systems. The classification into Seyfert 1 or 2 (Seyfert 1: broad permitted lines and Seyfert 2: narrow permitted lines) then depends on the inclination angle and hence on whether we can see the BLR. Although the concept of the unified model existed before the discovery by Antonucci & Miller (1985) of broad  $\text{H}\alpha$  emission in spectropolarimetry of the nearby luminous Seyfert 2 galaxy NGC1068, that result was seen by many as the major confirmation of the likely validity of the model. Although other Seyfert 2’s have also been found to have broad permitted lines in scattered light, this is by no means universal. Indeed Heisler, Lumsden & Bailey (1997) found a strong correlation between the ‘warmth’ of the IRAS  $60\mu\text{m}$  to  $25\mu\text{m}$  ratio and the

ability to detect such scattered broad-line radiation. Further studies that enhance our understanding of why some Seyfert 2s appear consistent with the unified model and others do not are clearly therefore of value.

In this context, infrared polarimetry of AGN provides valuable extra constraints on the polarisation mechanisms active in Seyfert 2’s. Since the unified model infers the presence of a dusty torus obscuring the AGN core, we might expect that longer wavelength polarimetry will be able to probe deeper into regions within the plane of the torus. Hence infrared polarimetry may let us see scattering in Seyfert 2’s which is otherwise shielded from view. In addition, many Seyfert 2’s with generally ‘warm’ IRAS colours are known to have polarisation rising into the near infrared (Young et al. 1996a). The mechanism generally invoked to explain such behaviour is linear absorptive dichroism, in which aligned dust grains preferentially absorb one plane of

polarisation. When such dust screens a bright background source, the transmitted light is therefore polarised. As shown by Hildebrand (1988), observations of this aligned dust component at wavelengths where it emits as well as at wavelengths where it absorbs can be used to study the nature and geometry of the dust that so heavily obscures the AGN along our line of sight.

Since it is already known from the spectropolarimetric observations that NGC1068 contains a hidden type 1 core, has relatively high polarisation for a Seyfert 2 (Heisler, Lumsden & Bailey 1997), and has rising infrared polarisation (Young et al. 1995), it makes a perfect target in which to test these ideas. Its proximity (14.4 Mpc; Tully 1988) and luminosity also make it an ideal candidate.

There has already been considerable previous work on infrared polarisation in NGC1068. The most extensive early broad-band polarimetry data are reported by Bailey et al. (1988), who found a strong rising red continuum in the near-infrared polarised flux and evidence for a gradual change in the position angle of polarisation between the optical and near infrared. They explained these as a combination of polarisation by scattering and due to transmission of a strongly reddened background source through aligned dust grains. They also found a much more marked change in polarisation angle ( $\sim 70^\circ$ ) between 4 and  $5\mu\text{m}$  due to the same aligned grains being seen in emission at longer wavelengths. This large swing in polarisation is seen again in the spectropolarimetry of Young et al. (1995) who also included polarisation by aligned grains in their model, having found that scattering fitted the data well below  $1\mu\text{m}$  but was deficient beyond that wavelength in explaining both the polarised flux and the position-angle data.

In addition, Aitken et al. (1984) presented  $10\mu\text{m}$  spectropolarimetry, showing that the percentage polarisation remained constant through the  $9.7\mu\text{m}$  silicate absorption feature. This showed that the cause of the  $10\mu\text{m}$  polarisation could not be absorption by aligned dust grains, since that would have resulted in a rise in polarisation through the absorption feature. However, they were unable to decide between the other alternatives: emission from aligned, optically thick (since the silicate absorption feature seen is relatively weak) dust grains or polarised emission from the active core itself. The position angle of polarisation seen at  $10\mu\text{m}$  is consistent with that found by Bailey et al. (1988) at  $5\mu\text{m}$ .

A consistent picture has begun to emerge from all these results. The optical data near the nucleus can be explained by a combination of a dominant electron-scattering component and a lesser dust-scattering one. The near-infrared polarisation is a combination of electron scattering and the dichroic component modelled by Young et al. (1995). The longer wavelength data is then consistent with emission from aligned grains, since the emission and absorption polarisation position angles from the same grains are roughly orthogonal.

However, two aspects were clearly lacking in all of this work. Since much of the activity in NGC1068 occurs within 1–2 arcseconds of the nucleus, high spatial resolution observations are required to separate the different polarisation mechanisms that may be present. Some high-resolution imaging polarimetry has been published by Young et al. (1996b) but this was obtained in moderate seeing conditions. The only other imaging data that exists in the near

infrared is that of Packham et al. (1997), but the resolution of this data is  $\geq 1.2$  arcseconds. All other previously published data were acquired using aperture bolometer devices. The second major lack is imaging polarimetry in the mid-infrared. Without such data it is not possible to relate the observed near-infrared data to the behaviour at longer wavelengths with a high degree of confidence. We have therefore gathered high-resolution ( $\sim 0.5$  arcsecond), complete near- and mid-infrared imaging polarimetry of the central regions of NGC1068 using the AAT. In section 2 we give details of these observations, in section 3 we present the results of our observations, in section 4 we analyse these results in terms of possible polarisation mechanisms, in section 5 we discuss the dust distribution around the nucleus of NGC1068 and finally in section 6 we present our conclusions.

## 2 OBSERVATIONS

All of the data presented in this paper were obtained on the nights of 9, 10 and 11 August 1995 and 11 October 1997 at the Anglo Australian Telescope. The  $10\mu\text{m}$  data were acquired with the ADFA mid-infrared camera, NIMPOL (Smith, Aitken and Moore, 1994), which at the time used a  $128^2$  SiGa array, with a pixel scale of  $0.25''/\text{pixel}$ . A cold wire grid and a warm rotating CdS half-wave plate were used as the analyser for the polarimetry. We used a standard broad band 8– $13\mu\text{m}$  filter for the observations, and chopped and nodded  $\sim 20''$  to sky so that the object was always present on the array. Extended emission at  $10\mu\text{m}$  is sufficiently weak (eg Telesco & Decher 1988) that this poses no problems for the nuclear polarimetry. Approximately 7 hours of actual on-target data were acquired. The image is diffraction limited, and all data taken during non-photometric conditions have been discarded. We observed NGC1068 at airmasses ranging between 1.2 and 1.8.

The near-infrared data were obtained on the nights of 11 August 1995 and 11 October 1997 with the common-user camera IRIS, which uses a  $128^2$  HgCdTe array. A warm rotating half-wave plate and a cold beam-splitting Wollaston prism were used to obtain the linear polarimetry: the Wollaston allows for very efficient polarimetric observations, and also allows reliable data to be taken even in non-photometric conditions. Again the pixel scale was  $0.25''/\text{pixel}$ . The seeing was estimated at  $0.6''$  during these observations. After each cycle of four waveplate positions we nodded the telescope to a separate sky position since the galaxy is bright in the near infrared beyond the nucleus. Approximately 20 minutes of data were obtained on source at each of J, H and  $K_n$ . Conditions were photometric for the H and J band observations, and partly photometric for the  $K_n$  observation. The photometry given in Section 2 is derived solely from those frames taken when conditions were photometric. Unfortunately, the conditions meant that it was difficult to obtain good ‘sky’ frames to subtract from the data at  $K_n$  due to clouds reflecting thermal emission from the ground. The result is a higher than expected background noise level in the polarisation images. We therefore also observed NGC1068 at H and  $K_n$  on the night of the 11th October 1997 with the same setup to check our results. We obtained 16 minutes of on-source data at  $K_n$  and 8 minutes at H on this night. The seeing was good for the  $K_n$  data ( $\sim 0.75$  arcseconds), but poorer for the

H band data ( $\sim 1$  arcsecond). Conditions were photometric during this night. This is evident in a considerable decrease in the noise in the polarised flux images. The polarimetry derived from both dates is consistent within the errors.

Flux calibration for the mid-infrared data was obtained from matching observations of the mid-infrared standards BS6832 ( $\eta$  Sgr;  $S(10\mu\text{m}) = 197$  Jy), BS8636 ( $\beta$  Gru;  $S(10\mu\text{m}) = 933$  Jy) and BS7525 ( $S(10\mu\text{m}) = 93$  Jy), and has an estimated uncertainty of 10%. Flux calibration for the near-infrared 1995 data was derived from SA241–251 and for the 1997 data from HD24849 (Carter & Meadows 1995).

The polarimeters used with both IRIS and NIMPOL are very stable, and instrumental effects result in errors as low as 0.1% in polarisation and less than  $1^\circ$  in position angle. In order to check the performance of the system with IRIS we also observed standard stars of known polarisation, as well unpolarised standards and stars observed with a wire grid (of known polarisation properties) in the beam. This allows the zero-point of the position angle to be set. The resulting errors found were in line with the expected performance. For NIMPOL, the polarisation standard was the BN object in Orion, assumed to have a polarisation angle of  $118^\circ$  at  $10\mu\text{m}$ .

The near-infrared data were reduced as follows. The data were flat-fielded using dome flats. Offset sky frames (several arcminutes from the source) were obtained using the same setup as for the object data. The frames for each half-wave plate position were median-filtered to remove background sources. The resultant four sky frames (one for each half-wave plate position) were scaled to the median level of the sky within each group of four individual object frames, and the result subtracted from the object frames (this technique proved resilient to residual sky variations from tests carried out by subtracting sky from individual sky frames themselves, which could otherwise provide an unwanted additional background ‘noise’ signal in the final polarisation). The resultant images were then registered and combined into separate mosaics for each half-wave plate position. These final mosaics were combined to form Q and U Stokes images, and hence polarisation maps. This procedure is valid because of the dual-beam nature of the instrument. Variations in sky brightness, or transparency, are correctly allowed for because the frames are scaled when combined to form the Stokes parameters ensuring that the total flux is conserved in any image.

The raw  $10\mu\text{m}$  data is stored with the chop already subtracted but the corresponding nod position is removed later in software. The result is then properly sky subtracted. Flat fields were made from pairs of sky observations, one at high ( $\sim 1.6$ ) and one at low ( $\sim 1.0$ ) airmass, which were subtracted and normalised. The sky-subtracted, flat-fielded data were registered to remove any small shifts in the object position with time, since the telescope was tracking without guiding. The shift observed is only  $\sim 1$  arcsecond per hour. Frames in which the background increased by more than 50% compared to others in a given sequence were discarded. Such frames were generally affected by cloud. The final data were then grouped into Stokes Q and U parameters. Note that since NIMPOL uses a wire grid analyser and not a Wollaston prism, residual variations in atmospheric transparency can affect the final results. We tested for this by breaking the data into sequential blocks and compared the

results. We found no evidence that cloud affected any of the data used in the final images.

### 3 POLARISATION MAPS AND PHOTOMETRY

#### 3.1 The near-infrared data

The near-infrared polarisation maps are shown in Figure 1 and the corresponding polarised-flux images (being flux multiplied by degree of polarisation) are shown in Figure 2. We have derived an error estimate for the polarised flux from the scatter in the counts well away from the nucleus, and in Fig. 1 only plot polarisation points which lie more than  $3\sigma$  above the mean background level. The images shown are derived from the 1997 data for H and  $K_n$ , and from the 1995 data for J. It is worth noting that the centroids of the direct flux and polarised flux are identical at all three wavebands to within less than one tenth of a pixel (0.02 arcseconds).

The measured polarisation is given in Table 1. The errors are derived by measuring the polarisation on every individual subset of four half-wave plate positions. We note that the measurement in the small aperture is highly sensitive to factors such as seeing, telescope drift etc, and therefore has a much higher error than the other values quoted. The results are in reasonable agreement with both Bailey et al. (1988) and Packham et al. (1997). We believe that the differences found by Packham et al. between their data and that of Bailey et al. may be largely due to factors such as seeing variations. The core of the emission from NGC1068 is clearly strongly polarised, but the profile of this core is narrow, so the resultant measured polarisation in a small aperture is strongly dependent on factors such as seeing.

The most immediately obvious features present in Figure 1 are the centro-symmetric vector patterns characteristic of scattering seen both northeast *and* southwest of the core. This provides a direct constraint on the geometry of the central regions of NGC1068. Since two scattering cones are seen in the present data, but only one in the optical and UV, the counter cone must be hidden by an extended screen at shorter wavelengths. The only likely candidate for this screen is the disc of the galaxy. This implies that the cones in NGC1068 are definitely not aligned along the plane of the galaxy, in agreement with previous evidence that the northeastern cone illuminates the near side of the disc whereas the southwestern cone illuminates the far side (cf Figures 1 and 2 of Bland-Hawthorn et al. 1997). In particular, maps of the [OIII] emission show that the southwestern emission region vanishes behind the larger-scale molecular ring that surrounds the nucleus at a distance of about 1kpc, whereas the northeastern emission is clearly visible. The same phenomenon can also explain the asymmetry in the X-ray emission (Wilson et al. 1992).

The polarisation vectors are clearly evident spread in an arc between the common axis of the large-scale ionisation cones and radio emission (eg. Wilson & Ulvestad 1987, Evans et al. 1991; position angle  $\sim 30^\circ$ ) and that of the inner radio jet (eg. Ulvestad et al. 1987; position angle  $\sim 10-30^\circ$ ). Whether or not this is one single continuous structure is not absolutely clear from the present data, however, which hint at there being two preferred directions in which the scatter-

ers lie, coincident with the two axes of the large- and small-scale radio emission. Data from HST may be invaluable in determining the true situation.

Our data are in good agreement with the images presented by Young et al. (1996b). The ‘shadow’ they noted in their H band data is also present in our data. We plot the image profile along the  $45^\circ$  direction (ie along the long axis of the images in Fig. 1) in Figure 3 for J, H and K. Note that our sign convention is opposite to that of Young et al., since positive offsets here are in the same sense as in Figure 1. In Fig. 3 we have used the H band data from 1995, when the seeing was better than for the 1997 H band data. The K band data from both 1995 and 1997 are consistent, but we show the former to ensure consistency with the other plots. The clear dip in the profile seen at J and H at an offset of  $\sim 1$  arcsecond agrees well with the H band profile plotted by Young et al. along a slightly different position angle. They attributed this to the possible shadowing of the scattering region by the torus. This is consistent with the presumed orientation of the ionisation cones if the torus is also aligned in the same sense.

Photometry in the three wavebands from both the August 1995 and October 1997 data are given in Table 2. Errors are estimates based on the scatter between the frames obtained. The larger error on the  $K_n$  data from August 1995 reflects the fact that not all of the data were photometric. For the 1997 data, we used all of the  $K_n$  data but only the first two minutes of the H band data since the seeing deteriorated after that point (clearly visible from the change in the individual image profiles). We have used only data taken in seeing better than 1 arcsecond. Because of the limited field of view, it is difficult to judge if the sky has been fully corrected for in these images. Light from NGC1068 dominates the images at all wavebands. We have adopted an average correction for the sky based on the detected counts 10 arcseconds from the nucleus. If this is an overcorrection, the tabulated fluxes will increase by less than 5%.

We can compare these results with those of Glass (1995), who published photometry over a twenty-year timespan in a 12 arcsecond aperture. There are several preliminary corrections that need to be made, however. Glass used a standard single-element photometer so that only 12 arcsecond aperture data is published. Because of the mask used in the imaging polarimetry our data is restricted to a 6 arcsecond aperture at most. Since NGC1068 varies slowly with time in the near infrared (Glass 1995), we cannot compare our data directly with other existing photometry. However, we can use such photometry to derive an estimate of the flux within a smaller aperture from the Glass data. We compared the Glass data at Julian date 2446314 with that from Bailey et al. (1988) in a 6-arcsecond aperture at  $JD \sim 2446450$ . This is a sufficiently small separation in time that the variability should be negligible. We ascribed the difference to emission in the annular ring between 3 and 6 arcseconds radius from the peak. As noted by Glass, the source that varies has the colours of hot dust: it is essentially the same as the bright core seen within 2 arcseconds of the nucleus in our images. It is likely, therefore, that the annular ring has little or no variability in flux, since it lies outside the hot-dust emission region. Assuming this is correct, we can subtract the derived annular flux from later data from Glass (JD 2449615) which is closer in time to our August 1995 data. Using this approx-

imation we derive a 6 arcsecond aperture flux density from the Glass data of 761mJy for K, 363mJy for H and 198 mJy for J. The errors on these numbers are entirely limited by the systematics of the approximations made, but it is likely that these values are reliable to within 10%. The results are in good agreement with our own 1995 data.

We can also compare our photometry with that of Packham et al. (1997). Their H band result would agree with ours if we made no additional sky correction. Their K band result is discrepant with our data even if we make this assumption (their result being  $\sim 400$ mJy brighter than the value given in Table 2).

Lastly, we note that the 1995 and 1997 data are in reasonable agreement with each other, and provide no strong evidence for a large change in brightness at these wavebands over this time period. Glass (1997) has reported that NGC1068 may now be declining in brightness at near-infrared wavelengths, although the magnitude of the decrease is small and roughly consistent with our own results.

### 3.2 The mid-infrared data

The  $10\mu\text{m}$  image is shown in Figure 4. The effective diffraction limit of the AAT at  $10\mu\text{m}$  is  $\sim 0.6''$ , and the dust emission is clearly not a point source. The data also clearly show that the polarisation structure arises from an extended region (all points with a signal-to-noise ratio greater than 5 in the polarisation are shown). In addition, there is a trend for the polarisation to increase away from the peak of the flux. The position angle of the polarisation is essentially constant across the region within the errors at  $55^\circ \pm 10^\circ$ . The measured aperture polarisation is given in Table 1.

Aitken et al. (1984) obtained aperture spectropolarimetry at  $10\mu\text{m}$  of the nucleus of NGC1068, showing a relatively featureless polarised flux spectrum. They concluded that the likeliest cause was emission from warm aligned dust grains, but could not rule out emission from the active nucleus itself. However, their data conclusively rule out an origin for the polarisation in absorption by dust since this would give a peak in the percentage polarisation through the silicate absorption feature at  $9.7\mu\text{m}$ . The result they derived was  $1.39 \pm 0.09\%$  polarisation at a rather poorly defined position angle (measured on two separate occasions at  $44.1 \pm 3.2^\circ$  and  $59.4 \pm 2.2^\circ$  in a 4.2 and 5.6 arcsecond diameter aperture respectively). Our observed position angle is consistent with the latter, though the measured polarisation is slightly higher in the 4.5 arcsecond aperture.

Dust emission can be seen up to  $5''$  from the nucleus, with the extended emission largely aligned with the observed ionisation cones (the inner high contours are also aligned with this direction as noted previously by Braatz et al. 1993). The measured flux density within a central 6 arcsecond aperture is  $24.7 \pm 2.1$ Jy, and within a 10 arcsecond aperture  $26.0 \pm 2.2$ Jy. The surface brightness at the lowest contour in Fig. 4 is  $\sim 100$ mJy/sq. arcsecond.

## 4 ANALYSIS

### 4.1 Polarisation mechanisms and the location of the AGN core

Young et al. (1995) found the dominant contribution to the polarisation at short wavelengths ( $\lambda < 1.5\mu\text{m}$ ) is from scattering (mostly from electrons). We can check this by examining the deviation from the expected centro-symmetric scattering pattern. As shown by Capetti et al. (1995), if only scattering is present then the average of the differences between the observed position angle in any pixel and the expected position angle (which is just the normal to the vector joining that pixel and the central source from which light is scattered into our line of sight), should be zero. Of course, this is a semi-iterative process since the exact location of the scattering centre is *a priori* unknown. However, it is trivial to iterate towards a solution for both the source of the scattered light and the deviation from the expected centro-symmetric pattern.

Figure 5 shows the observed departure from a pure-scattering vector pattern for all three wavebands. It is clear that the deviation in the expected vector pattern reaches a maximum at position angle  $\sim 115^\circ$  (ie for vectors with predicted position angle of  $30^\circ$ ) at all wavelengths. The observed pattern is consistent with that expected if polarised flux with a constant position angle were superposed on the observed scattered flux (see Section 4.2). Indeed this pattern is clear from Figure 1 as well. Only by masking out a region 2 arcseconds in radius around the central nucleus do we actually see no deviations from the expected scattering pattern. It is clear therefore that another mechanism contributes to the observed polarisation *at all wavebands*.

We masked out all the data within 2 arcseconds of the peak when deriving the actual scattering centre because of this additional mechanism that contributes near the nucleus, as well as those data with signal-to-noise ratio in the polarised flux less than  $3\sigma$  above the mean background. We found we could not determine the location of the scattering centre reliably by projecting orthogonal vectors back from the polarisation vectors to find a common centre. Residual background results in a ‘blurring’ of the polarisation position angles, so that some of the points of intersection lie well away from the nucleus. We therefore calculated, for each pixel in turn, the difference between the observed position angle and the position angle expected if that pixel were the centre. We then found the global minimum of this function, and this position is the scattering centre. This is far more stable to the effects noted, but at the cost of giving a less precise solution than would be possible with the other method given better data. This technique gave offsets from the respective flux centroids of  $0.11 \pm 0.18$ ,  $0.09 \pm 0.21$  and  $0.34 \pm 0.39$  arcseconds at J, H and  $K_n$  respectively, which are all formally consistent with no offset.

We note that Marco, Alloin & Beuzit (1997) found the centroid of the K band flux tentatively aligned with the location of the UV scattering centre (Capetti et al. 1995), and the radio sources S1 and S2 (Gallimore et al. 1996), from astrometry obtained using adaptive optics and offsets between the peaks of the optical and IR light. Our results are therefore entirely consistent with their analysis. We note that their result depends on determining a difference between the position of the peak of the I band light and the peak of the

K band light. Although it might seem unusual that the peak of the J band light should therefore be coincident with the peak of the K band light (since I is closer to J in wavelength than J is to K), the reason is simple. The J band centroid is dominated by the same polarised core that is seen at H and K even though the contrast with the electron scattering cones is much less. The same feature is unlikely to appear at I, as is clear from Section 4.2. It is the centroid of this feature that determines the location of the AGN core as we show below.

Lastly, we consider the factors that may affect our solution. These are systematic global position angle errors, random position angle errors and the role of seeing. Systematic global errors in the position angle calibration are constrained to be  $< 1^\circ$  from observations of polarised standard stars, which results in an entirely negligible change in the location of the scattering centre. We checked for effect of random position angle errors using a Monte-Carlo analysis of our observed data, drawing a new set of position angles from the set by randomly shifting the angle consistent with the observed error in the position angle. This had a negligible effect on the location of the centre. The effect of seeing is to blur the scattering pattern, especially near the bright nuclear continuum source. We have attempted to quantify this by simulating a simple ionisation cone irradiated by a centrally peaked Gaussian source, with noise levels throughout consistent with our data. This pattern was then smoothed to mimic the observed seeing, and rederived the polarisation from the model Stokes Q and U images. The result shows that seeing effects the observed pattern only in the inner 0.5 arcseconds around the flux centroid. Since we exclude this data anyway, seeing clearly has little affect on our result either. Therefore we can be confident that our result is correct, and that the scattering centre is coincident with the K band flux centroid.

### 4.2 The nature of the polarised core

As indicated by the analysis above, there is at least one other polarisation mechanism present within  $\sim 1 - 2$  arcseconds of the peak of the flux. Young et al. (1995) originally proposed that this was absorptive dichroism on the basis that no scattering law appeared to fit their spectropolarimetry. That suggestion was consistent with the results of Bailey et al. (1988) who also concluded that the cause of the  $\sim 70^\circ$  change in position angle between the near infrared and the mid infrared is the switch from emission to absorption by aligned grains as wavelength decreases. A lower limit to the temperature of the dust providing the screen can be set by the observation of Bailey et al. (1988) that the position angle of polarisation changes somewhere between 4 and  $5\mu\text{m}$ , from which we conclude that  $T_{\text{dust}} \gtrsim 350\text{K}$ .

The fact that the change in polarisation position angle is not closer to  $90^\circ$  may indicate one of two possibilities: first that the background source seen at  $\lambda < 4\mu\text{m}$  contributes to some extent at  $10\mu\text{m}$  too but is polarised itself with a different position angle (so at short wavelengths, the position angle is determined by the combined effects of dichroic absorption and polarised emission from the background, and at  $10\mu\text{m}$  from emission from both); second, that there is yet cooler dust that is still shielding the  $10\mu\text{m}$  emission, so that the observed position angle is a blend of the emission and

absorption processes (one test of this may be obtained by determining the polarisation in the sub-mm regime).

All our data are consistent with the background source being hot dust with temperatures near the sublimation point (see below), where grains are unlikely to be aligned by a magnetic field. Therefore *if* the grains are aligned by a magnetic field, the first possibility is ruled out. Alternative mechanisms such as alignment due to radiation pressure in the ionisation cone may give rise to a similar pattern (eg radiation pressure: Dopita et al. 1998) but it is difficult to see how these can give rise to alignments in both hot ( $> 1000\text{K}$ ) and warm/cool ( $\lesssim 400\text{K}$ ) dust components. It is also known that NGC1068 has a prominent silicate absorption feature at  $9.7\mu\text{m}$  (Roche et al. 1984), indicating the last explanation may be the most probable. If it is true, we would predict that the observed position angle may change through the silicate absorption feature from the  $45^\circ$  measured at  $5\mu\text{m}$  by Bailey et al. to the  $\sim 55^\circ$  we measure. Unfortunately the data of Aitken et al. (1984) are not sufficiently accurate to measure such small shifts.

We have modelled the wavelength dependence of the observed polarised flux in the core. The model is simple and assumes only three parameters that are allowed to vary. These are the temperature of the dust,  $T_{dust}$ , the emissivity of the dust (assumed to vary as a power law,  $\lambda^{-n}$ ), and the extinction to this dust source as measured in the K band,  $A_K$ . The polarised flux is assumed to be represented by an optically thin grey body with this temperature and emissivity, scaled by an appropriate Serkowski polarisation law (Serkowski, Mathewson & Ford 1975 and references therein) and then reddened using a standard  $\lambda^{-1.75}$  extinction law. The Serkowski law has the form

$$p(\lambda)/p_{max} = \exp[-K \ln^2(\lambda_{max}/\lambda)]$$

where we have adopted ‘typical’ values for moderately extinguished sources in our galaxy (Whittet et al. 1992) of  $K = 1.15$  and  $\lambda_{max} = 0.6\mu\text{m}$  (the effect of changing  $\lambda_{max}$  and  $K$  is small for the wavelength range of interest).

The results are indicative only given the few data points we are trying to fit. It may be possible, given small aperture spectropolarimetry between 1 and  $4\mu\text{m}$ , to provide better discrimination between the models. However, a typical ‘good fit’ to the data can be obtained with the following parameters:  $T_{dust} = 1200_{-200}^{+300}$ ,  $n = 1.5 \pm 0.5$  and  $A_K = 1.5 \pm 0.5$  (or  $A_V = 17 \pm 6$ ). The errors given here are not formal uncertainties but represent the range of values that produce reasonable fits to the three data points. The results are also correlated in the sense that larger  $n$  gives lower values of  $T_{dust}$ , and larger values of  $A_K$  require larger values of  $T_{dust}$ . However, it is clear that an extinguished hot dust source can explain the observed data. Since we might expect the hottest dust present to be near the sublimation temperature, the ‘likeliest’ parameters are those with high  $T_{dust}$  and  $A_K$  (ie  $T_{dust}=1500\text{K}$  and  $A_K = 2$ ).

We also considered a simple power law for the underlying source rather than a grey body. A reasonable fit can again be derived with similar  $A_K$  assuming the underlying source varies as  $\lambda$ , which, however, is inconsistent with typical synchrotron spectra. For the dust temperature derived, there is essentially no flux below  $1\mu\text{m}$ , explaining why and J and  $K_n$  centroids are similar to each other, and not to I band data.

We can estimate what fraction of the total flux at J within a 3 arcsecond aperture arises from the dust assuming the model with both large  $T_{dust}$  and  $A_K$  is correct. If we use the result of Thatte et al. (1997) that dust contributes 90% of the direct flux at K, and our model above, we predict that dust will contribute  $\sim 50\%$  of the total flux at H, and  $\sim 10\%$  at J. This is in agreement with our findings in Section 4.1 that even at J there is a source of polarisation other than scattering, and that the J flux centroid is coincident with the K flux centroid, since the centroids at both wavebands are determined largely by the centrally peak dust component. The same hot dust contributes similar flux density at 2 and  $10\mu\text{m}$ , or  $\sim 5\%$  of the total at  $10\mu\text{m}$ . Since in reality there will be a continuous range in dust temperature with distance from the source, it is likely that up to 25% of the  $10\mu\text{m}$  emission can come from dust hotter than 1000K.

Lastly, we can obtain an estimate of the position angle and dimensions of the inner regions of the obscuring material from our data. The position angle of the symmetry axis of this ‘torus’ is  $\sim 30^\circ$  ( $90^\circ$  from the deviation in the scattering pattern shown in Figure 5). This agrees well with previous estimates of the position angle of the torus (Young et al. 1995, 1996b, Miller et al. 1991), and of the large-scale radio emission (Wilson & Ulvestad 1987). The observed data are also marginally suggestive of an extended source aligned perpendicular to this, since the profiles along this direction and along the cone differ in extent by  $0.1 \pm 0.05$  arcseconds.

To derive better estimates of the size of the resolved inner-torus region we created a simple model in which a polarised core was superposed onto background scattered emission. The relative strengths of the core and background were taken from the actual  $K_n$  data. The polarisation was also taken from the observed data. We then convolved this model with the observed seeing. The resultant polarisation maps, though highly idealised, could be compared with the data to determine the actual extent of the polarised core. The results indicate that this region has approximate extent  $7 \times 15\text{pc}$ . We show in the next section that this extent is consistent with the observed mid-infrared emission from the ionisation cones. Clearly, high spatial resolution ( $\sim 0.1\text{arcseconds}$  or better) IR imaging polarimetry that can sample the fine structure in this region is desirable to estimate the true size of the torus.

### 4.3 Mid-infrared emission

As shown by both Braatz et al. (1993) and Cameron et al. (1993), it is possible to relate the observed dust temperature and its distance from the heating source to the source luminosity, after making suitable assumptions about the grain properties and assuming that the dust sees the source directly). Cameron et al. derive the following equation, assuming an emissivity proportional to  $\lambda^{-1.5}$ :

$$\left(\frac{R}{0.14\text{pc}}\right) = \left(\frac{0.05\mu\text{m} \times L}{a \times 1.5 \times 10^{11} L_\odot}\right)^{0.5} \left(\frac{T_{dust}}{1500\text{K}}\right)^{-2.7}.$$

Here  $a$  is the grain size in microns,  $L$  is (effectively) the luminosity of the core and  $T_{dust}$  the dust temperature. Clearly, for fixed  $R$  and  $L$ , the observed dust temperature is weakly inversely proportional to the grain size. Therefore, we might expect that it is the physically smallest grains (with

radii  $\sim 0.005\mu\text{m}$ ) that give rise to the hottest dust emission at any point and we adopt this factor in the following analysis.

First we consider the dust in the ionisation cone. Although we do not have an estimate of the dust temperature in the ionisation cones, we can assume a lower limit, which then gives a lower limit to the luminosity. The fact that we see dust emission at all at  $10\mu\text{m}$  implies  $T_{dust} \gtrsim 150\text{K}$ , just from a consideration of the sharpness of the drop in flux density with wavelength of a suitable grey body. If this dust is radiatively excited by the nucleus, this implies that the dust in the ionisation cones sees a luminosity of at least  $\sim 3 \times 10^{11} L_{\odot}$ . This is a factor of two higher than the estimated bolometric luminosity along our line of sight and may indicate anisotropic emission. This is not a new conclusion; Miller et al. (1991) found that the properties of the electron scattering region were also consistent with anisotropic emission from the core, as did Young et al. (1997).

Returning to the issue of the compact hot-dust emission discussed above, we see that for the same parameters, dust can be heated to 600K at a distance from the core of 8pc. Note we assume a lower limit to the temperature for the marginally ‘extended’ emission at K, since the 1500K dust visible at all three near infrared wavebands is likely to be an unresolved point source in our data (there is no visible extent at H and J so we cannot apply this analysis). Given the many assumptions that have gone into this simple analysis, the fact that this distance agrees with the limits set by our data is highly encouraging. The more extended dust around the nucleus should be dealt with using a proper radiative transfer model, since the source is likely to be screened by the hotter dust in that case (cf Pier & Krolik 1993, Efstathiou et al. 1995). It is interesting to note that the same parameters predict a dust temperature of approximately 100K at the radius of the large scale molecular ring seen in CO band images of NGC1068, which may just be warm enough to explain the excess  $10\mu\text{m}$  emission seen in that ring coincident with the ionisation cones (Bland-Hawthorn et al., 1997).

We modelled the observed  $10\text{-}\mu\text{m}$  polarisation structure as a combination of a point source (a reasonable approximation for the hot dust) and an extended component (warm dust). We assumed that the point source was completely unpolarised. The same results are obtained if the point source is polarised along a different axis to the extended component however. We convolved the point source with a suitable Airy function and subtracted this profile from the  $10\text{-}\mu\text{m}$  data until the percentage polarisation was constant across the nucleus. The best results are obtained if we allow the point source to have peak height 25% of the observed peak flux. The resulting polarisation pattern after subtraction then has  $p \sim 1.4\%$ . This result is also consistent with that expected from the model outlined in Section 4.2, where we found that between 5 and 25% of the emission at  $10\mu\text{m}$  could arise in dust at temperature greater than 1000K (ie dust where the alignment is likely to be destroyed).

## 5 COMPARISON OF MID AND NEAR INFRARED DATA

Young et al. (1995) modelled the polarised core of NGC1068 as arising due to absorptive dichroism, with an extinction to the emitting source of  $A_V \sim 45$ . However, this was based on the assumption that the contribution of the dust to the continuum emission seen in their  $3'' \times 3''$  aperture is  $\sim 15\%$  at H, whereas Origlia et al. (1993) estimate this contribution is  $\sim 30\%$  (in a slightly larger aperture) and Thatte et al. (1997) derive an estimate of  $65 \pm 5\%$  within a similar sized aperture. At K, Thatte et al. find that dust contributes  $89 \pm 5\%$  of the light within the same aperture, which is also larger than the value given by Origlia et al. (70%) within a slightly larger aperture. It is worth comparing these values with the crude estimates derived in Section 4.2. There we found  $\sim 50\%$  of the total H band light should be due to dust which is midway between the Thatte et al. and Origlia et al. estimates, but given the crudity of our procedure probably consistent with both. Packham et al. (1997) also estimated the required  $A_V$  to explain the observed data using a similar method to that given below, though placing the emphasis on the residual polarised flux after scattering had been allowed for, and derived  $A_V \sim 35$ . It is useful to consider this problem independently of the ‘best fit’ scattering model to see what limits can be placed.

The shape of the near-infrared spectrum is very sensitive to the dust temperature, assumed emissivity and extinction to the emission region as shown in Section 4.2. As noted there, changing any of these parameters has an effect on the others since they are correlated in any fit. It is therefore very helpful to derive independent estimates of any of these quantities. One method of deriving an independent estimate of the extinction is to compare the relative polarisation at  $10\mu\text{m}$  and K. The dust that shields the hot emission source evident in the K band is clearly cooler (and more spatially extensive from our  $10\mu\text{m}$  image) as noted above. As shown by Hildebrand (1988), the *intrinsic* percentage polarisation seen due to aligned dust grains both in emission and absorption can be related according to

$$p_{em} = p_{abs} / \tau_{\lambda(abs)},$$

if the result is taken at the same wavelength for both. This is clearly impractical, and a useful relation between absorptive polarisation at K and emissive polarisation at  $10\mu\text{m}$  must depend on the wavelength dependence of the dust cross-sections.

There are several other key assumptions in deriving a useful result from this simple relationship. First, it is assumed that scattering is not important at short wavelengths. This is true if we use a sufficiently small aperture near the peak of the flux at  $K_n$ , and at H to a lesser extent. It also assumes that the  $10\mu\text{m}$  emission is optically thin which is probably a reasonable approximation (note the fact that there is an observed silicate absorption feature as shown by Roche et al. (1984) does not violate this condition). The same grains must contribute at both wavelengths, and the wavelength dependence of the absorption/emission cross-sections are taken from the observed dependence of the known extinction law, from which  $\tau_K \sim 1.7\tau_{10}$ , and hence the same for the cross-sections. Therefore, we apply a correction of 0.6 to the observed  $K_n$  band polarisation.

We cannot use the observed values directly in this formula, since it relates solely to the properties of the dust. We can, however, correct these values, by estimating what fraction of the polarised light is due to scattering rather than dichroism, and what fraction of the direct light is due to stars rather than dust emission. For the former, we have derived aperture photometry on the polarised flux images within an aperture of diameter 3 arcseconds. We subtract off the extended contribution underlying the central source, assuming it is due to scattering (since this is where the scattered broad permitted lines arise). The result is assumed to be the polarised flux due to dichroic absorption of a background source. Of course, if the ‘background correction’ is not representative of the scattering properties near the core (for example, if the electron scatterers themselves are sharply peaked near the core) this will be an overestimate of the polarised flux due to dichroism. We can be confident this is not the case, however, just from the observed behaviour of the position angle of polarisation near the core. This essentially shows that within the innermost 1 arcsecond, scattering cannot dominate the light. The derived corrections are small for the region within 1.5 arcseconds of the core, and we find that 90 – 95% of the polarised flux in this region arises in the strongly peaked feature seen in Figure 3.

For the stellar contribution to the direct light, we use the values given by Thatte et al. (1997) but note that there appears to be an inconsistency between the results of Thatte et al. and Origlia et al. (1993). The difference in the result is small for the K-band data ( $A_V$  is  $\sim 3$  magnitudes larger), but significant if we use the H-band data. As a result we do not consider the H-band data in detail, but note that a similar result (in terms of  $A_V$ ) to that derived at K is obtained if we use the lower Origlia et al. value.

We also need to correct for possible extra sources that contribute to the  $10\mu\text{m}$  polarisation. As noted above it is possible that the hot dust contributes 25% of the light but none of the polarisation at  $10\mu\text{m}$ , and we have removed a point-source contribution at this level. The main uncertainty in the mid-infrared polarisation, however, is the dust opacity. Assuming the emitting regions are partially opaque implies that some of the emissive polarisation is itself absorbed as noted before. Hence the observed polarisation is actually reduced since the net effect of the absorption is to reduce the contrast between the axes of maximum and minimum polarisation (which is also the likely reason why the position angles are not orthogonal as noted in Section 4.2). Therefore, the result derived here should be thought of as an upper limit.

Therefore, assuming that  $p_{abs} \gtrsim 1.4\%$  and using  $p_{em} \sim 4.7\%$ , we derive  $\tau_K \lesssim 3.3$ , or  $A_V \lesssim 37$  assuming a standard IR extinction law. This sets the upper limit to the values the data allow. Since the estimated extinction to the AGN itself is  $> 80$  (Jackson et al. 1993), the cool dust is clearly only providing a fraction of the observed extinction. Our result is much larger than the observed optical depth in the silicate absorption feature (Roche et al. 1984 derive  $A_V \sim 8$ ), but reasonably consistent with the C-H band stretch absorption seen at  $3.4\mu\text{m}$  (Bridger et al. 1994 find  $A_V \sim 22$ ) the fits derived for the near-infrared polarised flux in Section 4.2 (where we found  $A_V \sim 23$  a reasonable fit) and the value derived by Packham et al. (1997) ( $A_V \sim 35$ ). The discrepancy with the silicate absorption feature is most likely

explained by infilling from the hot dust emission washing out the absorption feature, as shown by full radiative transfer models (Efsthathiou et al. 1995, Pier and Krolik 1993). Clearly therefore, if the hot dust is cospatial with the AGN core, then that dust itself must provide the bulk of the extinction to the core along our line of sight.

## 6 CONCLUSIONS

We have obtained new near- and mid-infrared imaging polarimetry of NGC1068. Our data are consistent with other observed results, but have generally higher spatial resolution than anything yet published. We can see clearly from our data that scattering alone fails to fit the observed data at all wavebands, and not just at K as noted previously by Young et al. (1995). We have shown how this deviation can be explained by absorptive dichroism of a background hot dust source, and find that at least part of the hot dust must have a temperature  $> 1000\text{K}$ . The screening dust must have temperature  $> 350\text{K}$ , since the observed change in position angle expected when moving from aligned grains emitting to aligned grains absorbing arises at  $\sim 4 - 5\mu\text{m}$ . It is likely that even cooler dust is also present which is shown only by the fact that the change in position angle in the infrared is not exactly  $90^\circ$ .

We have derived independent estimates of the extinction to the background hot dust source seen through the obscuring screen. The results, from fitting the observed near-infrared polarisation data and from comparing the near- and mid-infrared polarisation give results that are consistent with  $A_V = 20 - 40$ . This is considerably less than the estimate for the extinction through the observed molecular material to the AGN core itself (eg Jackson et al. 1993 find that  $A_V = 80$  from consideration of the optical depth observed in the circumnuclear molecular gas). The large visual extinction to the hot dust however explains why previous authors have noted the absence of a near-infrared excess in NGC1068 as typically seen in Seyfert 1’s (eg Edelson & Malkan 1986, Cameron et al. 1993). If the hot dust were unobscured, the combined spectrum of it and the more extensive warm dust would indeed peak near  $5\mu\text{m}$ . It may be that the hot dust component is actually the ‘classical’ torus, whereas the warm dust is distributed more widely and diffusely throughout the circumnuclear molecular clouds and the narrow line region. This is in line with the results of Heisler et al. (1997) who found a strong correlation between the size of the electron scattering region and the obscuring material in a sample of far-infrared selected Seyfert 2’s.

It is clear from our results that near-infrared polarimetry offers a potentially valuable insight into the nature of the obscuring material. In particular, it allows us to determine the properties of the warm dust that is nearest the AGN core. The clearest need for the future is high spatial resolution spectropolarimetry to define the polarisation behaviour as a function of wavelength, and for polarisation predictions to be included in radiative transfer modelling of the dust absorption/emission near AGN. The former will be especially useful when applied to techniques such as that discussed in Section 4.2, as well as greater information of the overall polarisation properties of dust absorption features, which may show weak features in the change in position an-



gle not previously considered. There is also clear scope for these methods to be applied to other nearby Seyfert 2s with warm far-infrared colours.

### References

- Aitken, D.K., Bailey, J.A., Briggs, G., Hough, J.H., Roche, P.F., 1984, *Nature*, 310, 660
- Antonucci, R., Miller, J., 1985, *ApJ*, 297, 621
- Bailey, J.A., Axon, D.J., Hough, J.H., Ward, M.J., McLean, I.S., Heathcote, S.R., 1998, *MNRAS*, 234, 899
- Bland-Hawthorn, J., Lumsden, S.L., Voit, G.M., Cecil, G.N., Weisheit, J.C., 1997, In Gallimore, J., Tacconi, L., eds, *The Proceedings of the Workshop on NGC1068*, *ApSS*, 248, 177
- Braatz, J.A., Wilson, A.S., Gezari, D.Y., Varosi, F., Beichman, C.A., 1993, *ApJ*, 409, L5
- Bridger, A., Wright, G.S., Geballe, T.R., 1994, in McLean, I., ed., *Infrared Astronomy with Arrays*, Kluwer, Dordrecht, p537
- Cameron, M., Storey, J.W.V., Rotaciuc, V., Genzel, R., Verstraete, L., Drapatz, S., Siebenmoregen, R., Lee, T.J., 1993, *ApJ*, 419, 136
- Capetti, A. Axon, D.J., Macchetto, F., Sparks, W.B., Boksenberg, A., 1995, *ApJ*, 446, 155
- Carter, B.S., Meadows, V.S., 1995, *MNRAS*, 276, 734
- Dopita, M.A., Heisler, C.A., Lumsden, S.L., Bailey, J.A., 1998, *ApJ*, 498, 570
- Edelson, R.A., Malkan, M.A., 1986, *ApJ*, 308, 59
- Efstathiou, A., Hough, J.H., Young, S., 1995, *MNRAS*, 277, 1134
- Evans, I.N., Ford, H.C., Kinney, A.L., Antonucci, R.R.J., Armus, L., Caganoff, S., 1991, *ApJ*, 369, L27
- Gallimore, J.F., Baum, S.A., O'Dea, C.P., 1996, *ApJ*, 464, 198
- Heisler, C.A., Lumsden, S.L., Bailey, J.A., 1997, *Nature*, 385, 700
- Hildebrand, R.H., 1988, *QJRAS*, 29, 327
- Jackson, J.M., Pagalione, T.A.D., Ishizuki, S., Nguyen-Q-Rieu, 1993, *ApJ*, 418, L13
- Marco, O., Alloin, D., Beuzit, J.L., 1997, *A&A*, 320, 399
- Miller, J.S., Goodrich, R.W., Mathew, W.G., 1991, *ApJ*, 378, 47
- Origlia, L., Moorwood, A.F.M., Oliva, E., 1993, *A&A*, 280, 536
- Packham, C., Young, S., Hough, J., Axon, D., Bailey, J., 1997, *MNRAS*, 288, 375
- Roche, P.F., Aitken, D.K., Phillips, M.M., Whitmore, B., 1984, *MNRAS*, 207, 35
- Serkowski, K., Mathewson, D.S., Ford, V.L., 1975, *ApJ*, 196, 261
- Smith C.H., Aitken D.K., Moore T.J.T., 1994, in Crawford D.L., Craine E.R., eds, *Proc. SPIE 2198, Instrumentation in Astronomy VIII*, SPIE, Bellingham, 2198, p. 736
- Telesco, C.M., Decher, R., 1988, *ApJ*, 334, 573
- Thatte, N., Quirrenbach, A., Genzel, R., Maiolino, R., Matthias, T., 1997, *ApJ*, 490, 238
- Tully, R.B., 1988, *Nearby Galaxies Catalog*, Cambridge University Press
- Ulvestad, J.S., Neff, S.G., Wilson, A.S., 1987, *AJ*, 93, 22
- Whittet, D.C.B., Martin, P.G., Hough, J.H., Rouse, M.F., Bailey, J.A., Axon, D.J., 1992, *ApJ*, 386, 562
- Wilson, A.S., Ulvestad, J.S., 1987, *ApJ*, 319, 105
- Wilson, A.S., Elvis, M., Lawrence, A., Bland-Hawthorn, J., 1992, *ApJ*, 391, L75
- Young, S., Hough, J.H., Axon, D.J., Bailey, J.A., Ward, M.J., 1995, *MNRAS*, 272, 423
- Young, S., Hough, J.H., Efstathiou, A., Wills, B.J., Bailey, J.A., Ward, M.J., Axon, D.J., 1996a, *MNRAS*, 281, 1206
- Young, S., Packham, C., Hough, J.H., Efstathiou, A., 1996b, *MNRAS*, 283, L1
- Young, S., Hough, J.H., Axon, D.J., Bailey, J.A., in Wickramasinghe, S., Ferrario, L., Bicknell, G., eds, *Accretion Phenomena and Related Outflows*, *ASP Conference Series* 121, 280

J band polarisation		
Aperture Diameter (arcsec)	Polarisation (percent)	Position Angle (degrees)
2	$2.25 \pm 0.25$	$106.8 \pm 2.0$
4.5	$1.59 \pm 0.15$	$105.3 \pm 1.0$
6	$1.35 \pm 0.10$	$103.9 \pm 1.0$
H band polarisation		
Aperture Diameter (arcsec)	Polarisation (percent)	Position Angle (degrees)
2	$3.87 \pm 0.20$	$117.0 \pm 2.0$
4.5	$3.06 \pm 0.10$	$115.0 \pm 1.0$
6	$2.58 \pm 0.05$	$114.5 \pm 0.5$
$K_n$ band polarisation		
Aperture Diameter (arcsec)	Polarisation (percent)	Position Angle (degrees)
2	$4.57 \pm 0.5$	$120.2 \pm 2.0$
4.5	$4.19 \pm 0.08$	$120.3 \pm 0.5$
6	$4.07 \pm 0.08$	$119.6 \pm 0.5$
N band polarisation		
Aperture Diameter (arcsec)	Polarisation (percent)	Position Angle (degrees)
2	$1.30 \pm 0.05$	$49 \pm 3$
4.5	$1.80 \pm 0.05$	$57 \pm 6$

**Table 1:** The measured polarisation within a circular aperture around the peak of the observed total flux.

Aperture Diameter (arcsec)	Flux Density (mJy)
J band photometry	
3	$93 \pm 10$
6	$198 \pm 10$
Aug. 1995 H band photometry	
3	$243 \pm 10$
6	$390 \pm 15$
Oct. 1997 H band photometry	
3	$240 \pm 15$
6	$420 \pm 15$
Aug. 1995 $K_n$ band photometry	
3	$650 \pm 30$
6	$800 \pm 30$
Oct. 1997 $K_n$ band photometry	
3	$553 \pm 20$
6	$785 \pm 10$

**Table 2:** The measured photometry for NGC1068 in a circular aperture around the peak of the flux.

## Figures

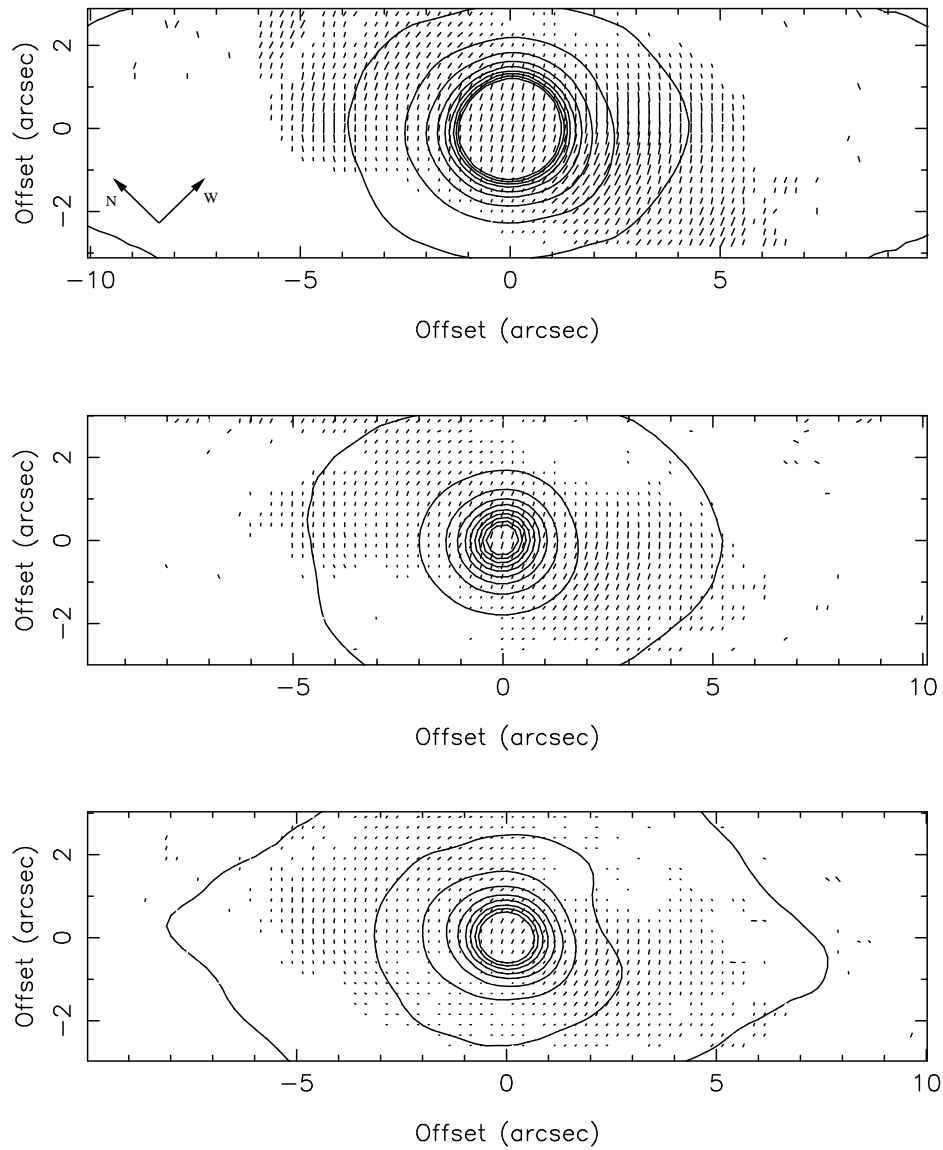


**Figure 1:** Near infrared polarisation maps of the nucleus of NGC1068. The  $K_n$  data are shown at the top, H in the middle and J at the bottom. A vector 1 arcsecond long represents 5% polarisation. The contours are of the total flux and are scaled arbitrarily.

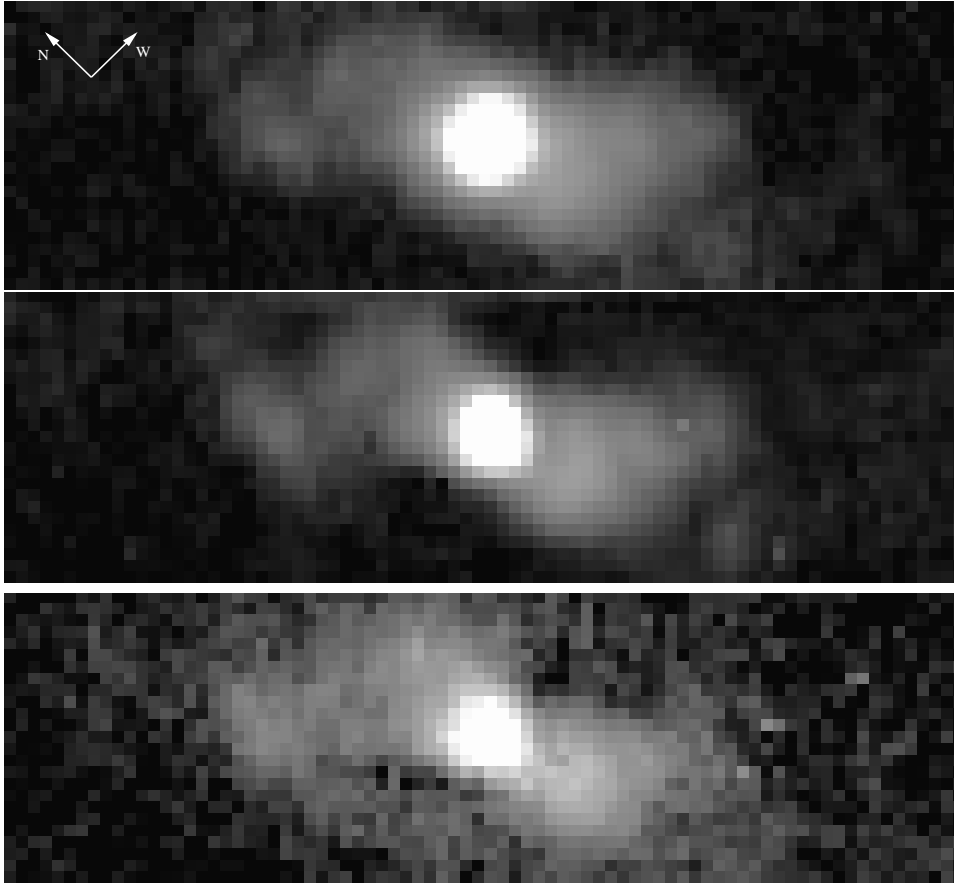


**Figure 2:** Near infrared polarisation images of NGC1068. The  $K_n$  data are shown at the top, H in the middle and J at the bottom. The scale is the same as in Figure 1.

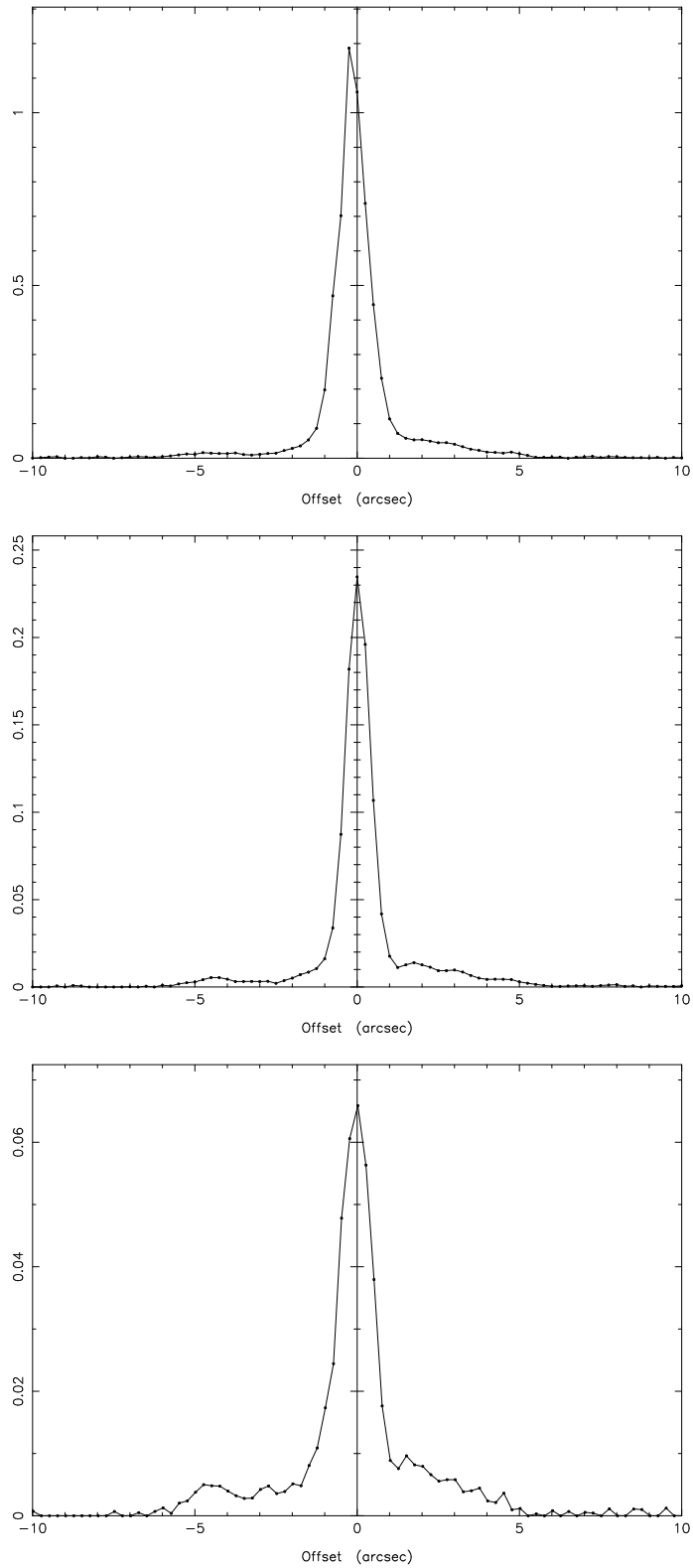


**Figure 3:** Cross section through the images shown in Figure 2. The  $K_n$  data are shown at the top, H in the middle and J at the bottom. The dip in the profile at  $-1$  arcsecond offset at H and J is the same as the feature reported by Young et al. (1996)

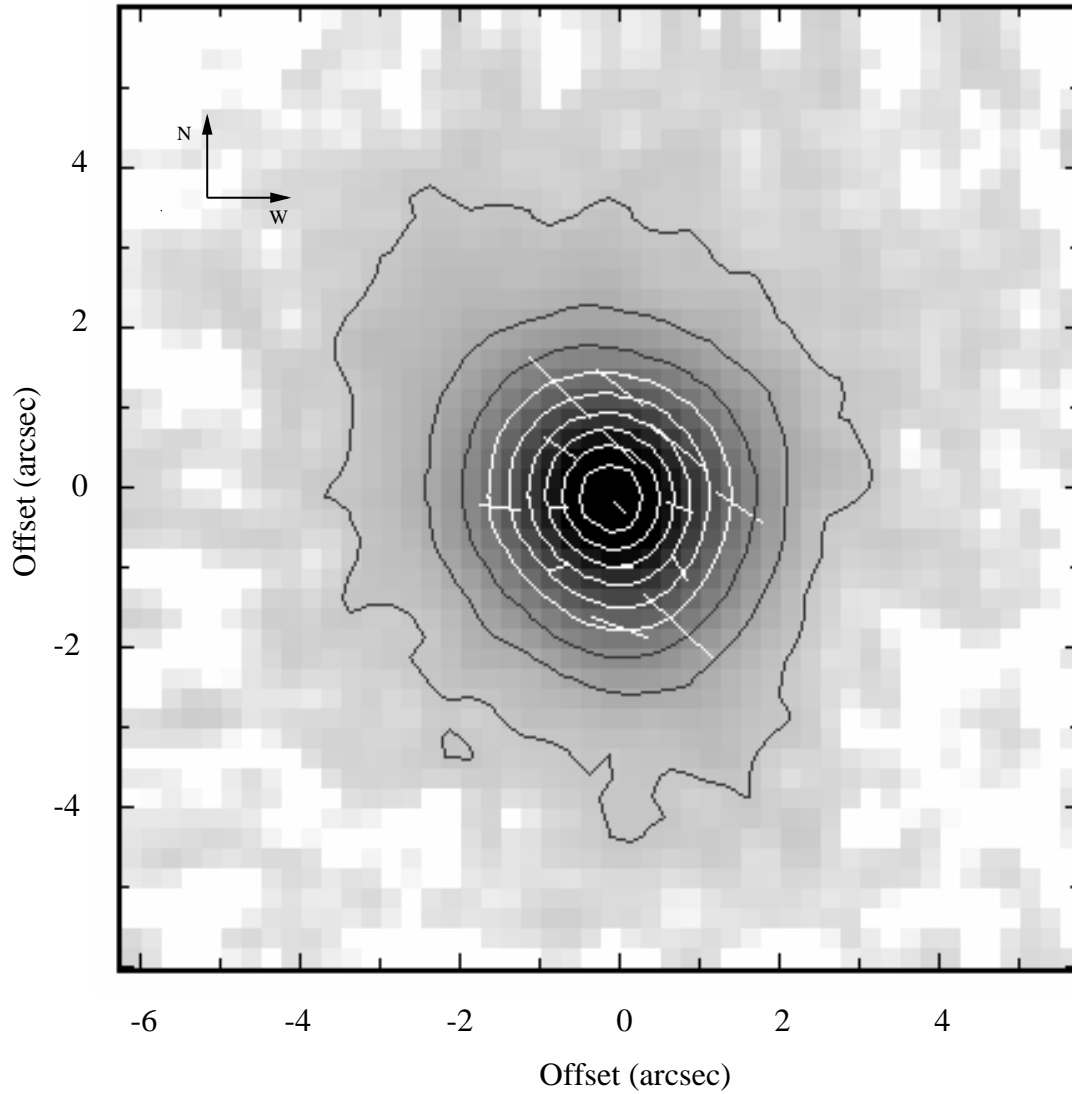


**Figure 4:** Mid infrared polarisation map of the nucleus of NGC1068. The data in the greyscale image have been smoothed slightly to enhance the contrast in the faint extended emission. The data are displayed on a power-law scale (surface brightness to the third power). The contours are evenly distributed in on the same scale, but are otherwise arbitrary.

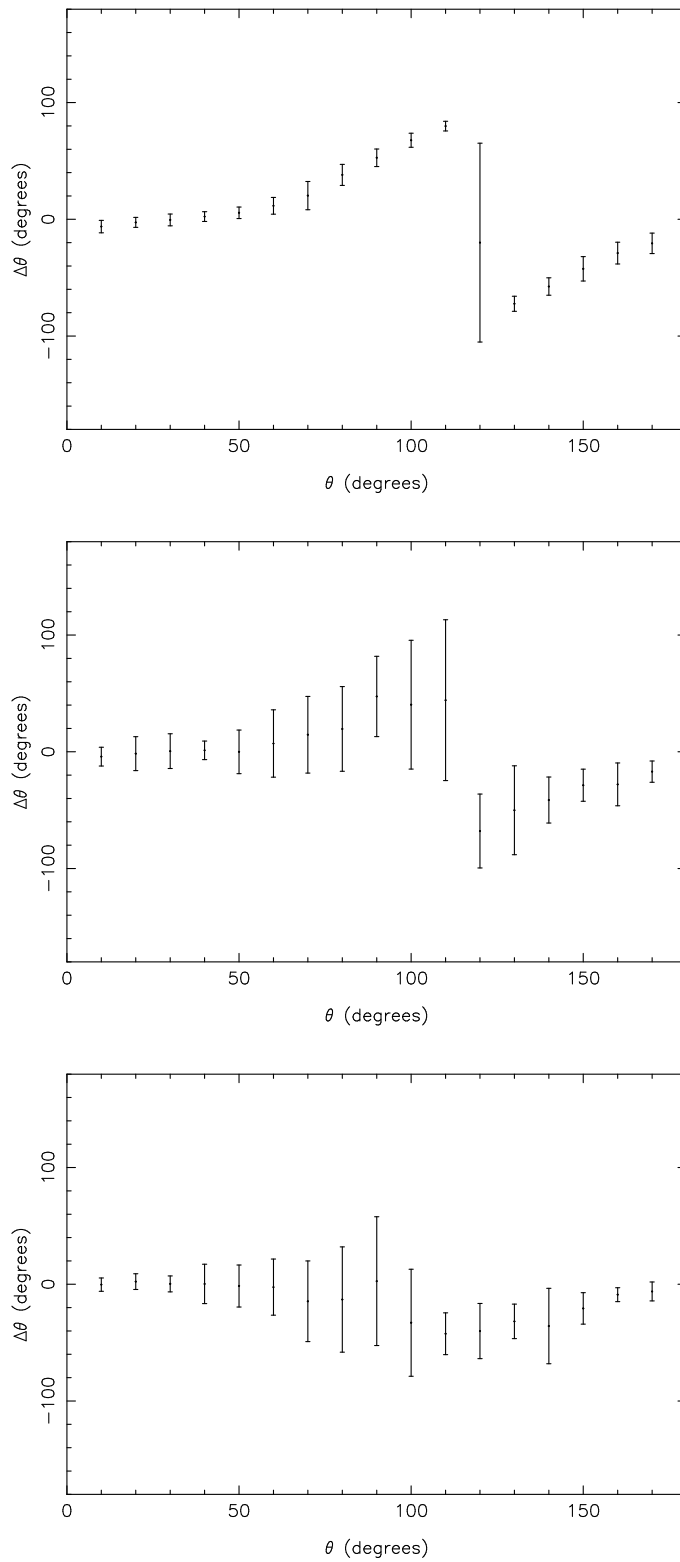


**Figure 5:** Deviation of the observed position angle of polarisation from that expected from a centro-symmetric scattering pattern. Pure scattering would be represented by a straight line through zero. Again, the  $K_n$  data are shown at the top, H in the middle and J at the bottom. The greatest departure from zero is always at approximately  $115^\circ$ . The width of this feature in the J band data is a reflection of the relative weakness of the additional polarisation component in this case.